Journal of Neurochemistry

JOURNAL OF NEUROCHEMISTRY | 2015 | 133 | 320–329 doi: 10.1111/jnc.13051

ORIGINAL ARTICLE

Ligand-directed delivery of fluorophores to track native calcium-permeable AMPA receptors in neuronal cultures

Rosamund E. Combs-Bachmann,* Jeffreys Nate Johnson,* Devaiah Vytla,*,† Amanda M. Hussey,† Maria L. Kilfoil‡ and James J. Chambers*,†

*Neuroscience and Behavior Program, University of Massachusetts, Amherst, Massachusetts, USA
†Department of Chemistry, University of Massachusetts, Amherst, Massachusetts, USA
‡Department of Physics, University of Massachusetts, Amherst, Massachusetts, USA

Abstract

Subcellular trafficking of neuronal receptors is known to play a key role in synaptic development, homeostasis, and plasticity. We have developed a ligand-targeted and photo-cleavable probe for delivering a synthetic fluorophore to AMPA receptors natively expressed in neurons. After a receptor is bound to the ligand portion of the probe molecule, a proteinaceous nucleophile reacts with an electrophile on the probe, covalently bonding the two species. The ligand may then be removed by photolysis, returning the receptor to its non-liganded state while leaving intact the new covalent bond between the receptor and the fluorophore. This strategy was used to label polyamine-sensitive receptors, including calcium-permeable AMPA receptors, in live hippocampal neurons from rats. Here, we describe experiments where we examined specificity, competition, and concentration on labeling efficacy as well as quantified receptor trafficking. Pharmacological competition during the labeling step with either a competitive or non-competitive glutamate receptor antagonist prevented the majority of labeling observed without a blocker. In other experiments, labeled receptors were observed to alter their locations and we were able to track and quantify their movements.

Keywords: AMPA receptors, calcium, fluorescent labeling, receptor trafficking.

J. Neurochem. (2015) **133**, 320–329.

Active trafficking of α-amino-3-hydroxy-5-methyl-4-isoxazolepropionic acid receptors (AMPARs) into and out of synapses is known to play a central role in the molecular mechanisms underlying learning, memory, and certain neuropathologies (Bennett *et al.* 1996; Tateno *et al.* 2004; Kerchner and Nicoll 2008; Ribrault *et al.* 2011). Our current understanding of these receptors is that the majority of functional heterotetrameric AMPARs contain edited GluA2 subunits and are thus impermeable to calcium (Isaac *et al.* 2007). These calcium-impermeable receptors function to mediate the majority of excitatory neurotransmission in the CNS. However, calcium-permeable AMPARs (CP-AMPARs) that lack GluA2 subunits have been found to be more populous and potentially more important than previously thought, and several recent reports describe the importance of this type of receptor in the fundamental framework of neural plasticity (Cull-Candy *et al.* 2006; Liu and Zukin 2007; Zonouzi *et al.* 2011; Rajasekaran *et al.* 2012; Sanderson *et al.* 2012; Szabo *et al.* 2012; Wolf and Tseng 2012; Yuan and Bellone 2013; Yuan *et al.* 2013; Morita *et al.* 2014). Moreover, while GluA2-containing heterotetrameric AMPARs are typically calcium-impermeable due to enzymatic editing of an mRNA codon that changes the code for a pore-lining residue from glutamine to arginine (Isaac *et al.* 2007), there is considerable evidence for expression of unedited, functional GluA2 subunit-containing AMPARs in developing neurons and in certain neuropathological diseases (Liu *et al.* 2004; Tateno *et al.* 2004; Corona and Tapia 2007; Corona *et al.* 2007; Bogaert *et al.* 2010; Hideyama *et al.* 2010; Kwak *et al.* 2010; Lee *et al.* 2010; Spaethling *et al.* 2012). Despite the demonstrated importance of CP-AMPARs

Received September 28, 2014; revised manuscript received January 15, 2015; accepted January 21, 2015.

Address correspondence and reprint requests to James J. Chambers, Department of Chemistry, University of Massachusetts, Amherst, 710 North Pleasant Street, Amherst, MA, USA. E-mail: chambers@chem.umass.edu

Abbreviations used: DNQX, 6,7-dinitroquinoxaline-2,3-dione; NAS, naphthylacetylspermine.

in synaptic function, plasticity, and disease, a simple non-electrophysiological method to study their expression patterns and dynamic movements is presently lacking.

Contrast agents such as fluorophores have traditionally been used to study protein localization in neurons. This is accomplished by either exogenous expression of a fluorescent fusion protein or recognition tag or by the application of a fluorescently labeled antibody to the protein of interest. While these methods are exquisitely sensitive for revealing the subcellular location of target proteins, they seldom reveal information on the activation state of ion channels and generally cannot provide information on the assembly characteristics of heteromultimeric ion channels.

Recently, we developed a small molecule (Nanoprobe **1**, Fig. 1) that is designed to label the subtype of CP-AMPARs receptors with a fluorescent tag in a traceless fashion through the use of a subtype-specific and use-dependent ligand. The ligand that we use is based on a class of wasp and spider toxins that all share a similar arylated polyamine pharmacophore. We have previously demonstrated via patch clamp electrophysiology that Nanoprobe **1** can block heterologously expressed CP-AMPARs in a use-dependent fashion when co-applied with glutamate but not in the absence of glutamate (Vytla *et al.* 2011). We have now used this targeting strategy to visualize native CP-AMPAR location and movements in hippocampal neuron cultures (days *in vitro*, DIV 14–17).

Materials and methods

Ethics statement

All animal care and experimental protocols were approved by the Animal Care and Use Committee at University of Massachusetts-Amherst, Amherst, MA, USA (IACUC Approval number 2012-0002). Animals were purchased as needed from Charles River Laboratories (Wilmington, MA, USA).

Dissociated hippocampal cell culture

Primary dissociated hippocampal cultures were prepared from embryonic day E19-20 Sprague–Dawley rat embryos and were cultured on polylysine-coated coverslips (12 mm, 1.0 size) in serum-containing medium identical to previous reports (Chambers and Kramer 2008). Cells were grown in an environment of 5% CO_2 at 37°C and were fed 200 μL of fresh media every 5 days.

Nanoprobe 1 labeling in neurons for live cell imaging

Coverslips of cells were mounted in a 12 mm perfusion apparatus (P-3, RC-25; Warner Instruments, Hamde, CT, USA) and were bathed in extracellular buffer containing 138 mM NaCl, 1.5 mM KCl, 1.2 mM $MgCl_2$, 5 mM HEPES, 2.5 mM $CaCl_2$ and 14 mM glucose at pH 7.4. To image fluorescently labeled receptors, coverslips of live neurons were washed three times with extracellular buffer to remove traces of serum, placed in fresh extracellular buffer, and imaged for 2 min to establish background fluorescence levels. The cells were then treated with test solutions containing either 20 μM glutamate and Nanoprobe **1** or 20 μM glutamate and Nanoprobe **1** with either 300 nM naphthylacetylspermine (NAS) or 10 μM 6,7-dinitroquinoxaline-2,3-dione (DNQX). After an incubation period of 5 min at 23°C in the dark, the coverslip was concurrently irradiated with 405 nm light for 15 s to result in photolysis of the nitroindoline while being washed three times with extracellular buffer (Trigo *et al.* 2009). Fresh extracellular buffer was then added and the cells were subsequently imaged.

Microscopy

Images of live neurons were acquired with a Nikon TiE microscope fitted with a CSU-x1 Yokogawa spinning disk confocal scan head

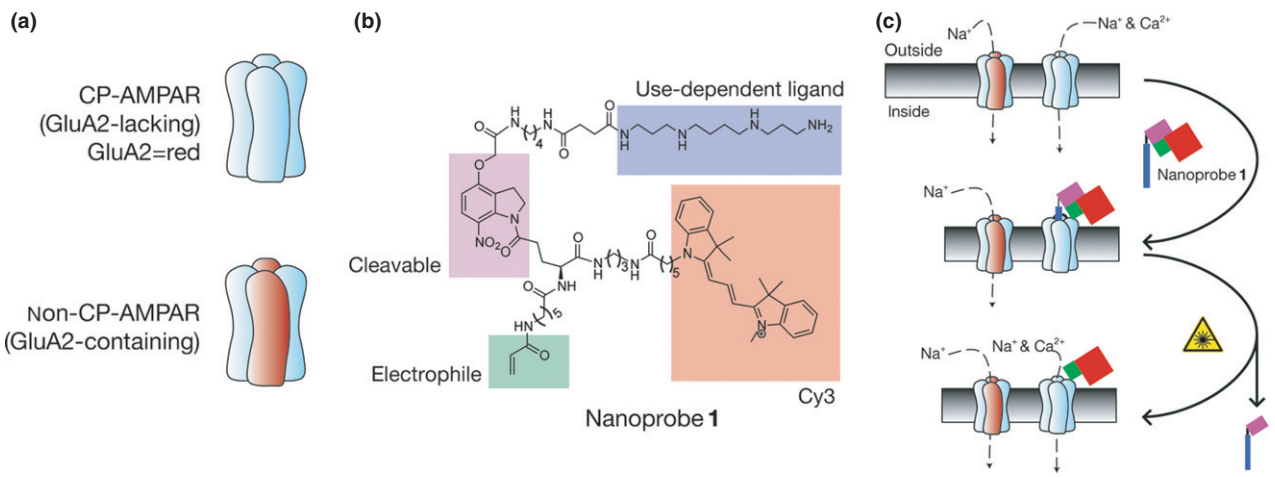

Fig. 1 CP-AMPARs and Nanoprobe **1** structure and function. (a) CP-AMPARs (all blue) are those that lack edited GluA2-subunits (red). (b) Nanoprobe **1** structure contains four components: a use-dependent polyamine ligand for targeting (blue), an electrophilic acrylate (green), a Cy3 fluorophore (red), and a photo-cleavable nitroindoline linker (purple). (c) Schematic depiction of use-dependent, phenotype-specific labeling of endogenous CP-AMPARs. After Nanoprobe **1** binds to and blocks the ion conduction pore of CP-AMPARs it can covalently crosslink via a Michael addition to the acrylate. Next, the ligand and nitrosoindole photoproduct may be removed with light to leave functional, Cy3-labeled CP-AMPARs.

(PerkinElmer, Waltham, MA, USA) and an Andor iXon+ electron-multiplying CCD camera (Andor, Belfast, Northern Ireland). All confocal microscope settings were kept identical for experiments in which labeling efficiencies were compared. The microscope and laser system was controlled by MetaMorph software (Molecular Devices, Sunnyvale, CA, USA) and we used a 100×/numerical aperture (NA) 1.4 objective for fluorescence and phase contrast imaging. 250 ms exposures of the 561 nm laser were used to detect and image Nanoprobe **1** labeling and this setting was well below pixel saturation. The size of each pixel in all of the acquired confocal images is such that the pixel is square and one pixel is 140 nm on each side.

Analysis

All images were analyzed using ImageJ (U.S. National Institutes of Health, Bethesda, MD, USA) (Schneider *et al.* 2012). To allow for quantification of Nanoprobe **1** accumulation, regions in the field of view which demonstrated fluorescence after glutamate/Nanoprobe **1** application (which occurs either after low dose or after pharmacological competition experiment) were identified by applying the Triangle threshold, a method to geometrically find the maximal data within the largest histogram range (Zack *et al.* 1977). These thresholded images were used as input for particle detection to generate an exhaustive ROI (region of interest) list of all labeled regions in the field of view. These ROIs were then applied to the previous time points for quantification of fluorescence during either low dose or competition incubations. Fluorescence intensities were quantified using the mean gray value of regions labeled with Nanoprobe **1**. Fluorescence intensity was then measured at these same regions for all previous and following time points. To correct for background fluorescence, three background ROIs were drawn where there was an absence of visible cells in the corresponding bright-field image. The mean intensity of these areas was used to calculate the average background that was then subtracted from the mean gray value of ROIs at each time point to determine background fluorescence before treatment, fluorescence after treatment with control (competition or low dose) solution, and fluorescence after treatment with Nanoprobe **1** alone. All brightness and contrast settings are equal within groups for comparative images presented in Fig. 2 except in the one case where indicated. Group mean values at each concentration (Fig. 2a) or treatment condition (Fig. 2c) were compared to the respective control values using a one-way non-parametric Kruskal–Wallis test (Mangiavacchi and Wolf 2004). The significant differences were further analyzed with Dunn's multiple comparison test. In all cases, $p < 0.05$ was considered statistically significant and individual p values are provided for each test. Asterisks in the figure represent statistically significant differences. The values on the graph are expressed as means ± 95% confidence interval unless otherwise noted.

Tracking data from experiments with DIV 14–17 neurons (Fig. 3) was generated with Matlab using a custom-built particle tracking software package (Pelletier *et al.* 2009). To detect the spots that were moving rapidly along neurites as well as those that were relatively stationary, we used a feature size of three pixels. Each image in the time series was initially filtered to suppress high frequency noise and low frequency background variations. The time series images were collected as a series of single z-plane images and thus, particles that move out of focus or into focus during the acquisition are either lost midway through tracking or commenced midway through tracking (Movie S2 demonstrates the effect of tracks being lost and started at different time points). The filtered image was then processed to find local intensity maxima, which are then used as estimated positions in integer pixels for the features sought. To refine the feature position about each local maximum, an area surrounding the estimated position of radius three pixels was extracted from the image, and the refined centroid position was used as the center for a second iteration of area extraction and centroid determination. This process yielded the final, calculated center position in two dimensions with a computed accuracy of 7 nm. To reliably find features in the face of photobleaching and consequent signal-to-noise degradation, the criteria for minimum integrated signal intensity and average signal intensity for each feature were adjusted automatically throughout the time series, following initial careful determination of appropriate acceptance criteria. We manually inspected the tracked particles toward the end of each time series to be certain we were robustly tracking particles that were easily visible. These criteria were then linearly adjusted to the initial frames of the time series so that particles with similar properties could be tracked in both early and late frames of each time series. Tracking in time can help discriminate noise from real features, as noise will typically not be spatially and temporally coherent. To define tracks and movements, the features that were found were allowed to move a maximum of eight pixels between frames and were required to be tracked for a minimum of 15 frames. The tracks were then overlaid onto the original time-lapse series and manually checked to confirm their acceptance as bona fide tracks.

Statistical analysis

Data are expressed as mean ± 95% confidence intervals. Static image data were processed with ImageJ and then analyzed using GraphPad Prism v5.0 (La Jolla, CA, USA). Significance was tested using a one-way non-parametric Kruskal–Wallis test. Significant differences were further analyzed with a Dunn's multiple comparison test. Dynamic movements of vesicles were processed and analyzed with Matlab r2013b (Mathworks, Inc., Natick, MA, USA).

Results

In neuronal cultures, we have found that Nanoprobe **1** labeling reveals an abundance of CP-AMPARs. These receptors can be detected at putative synaptic spines and can be observed to undergo local trafficking as well as active intracellular transport over the course of minutes. Control experiments using competitive molecules have demonstrated that the labeled proteins are likely CP-AMPARs as the majority of labeling is blocked either by competition with NAS or DNQX in these cultures.

To achieve CP-AMPAR specificity, the ligand portion of Nanoprobe **1** was designed to capitalize on the pharmacology of the polyamine toxin molecules Joro spider toxin, argiotoxin, philanthotoxin-433, and the synthetic CP-AMPAR blocker NAS (Brackley 1992; Stromgaard *et al.* 1999; Yoneda *et al.* 2001; Stromgaard and Mellor 2004). Each

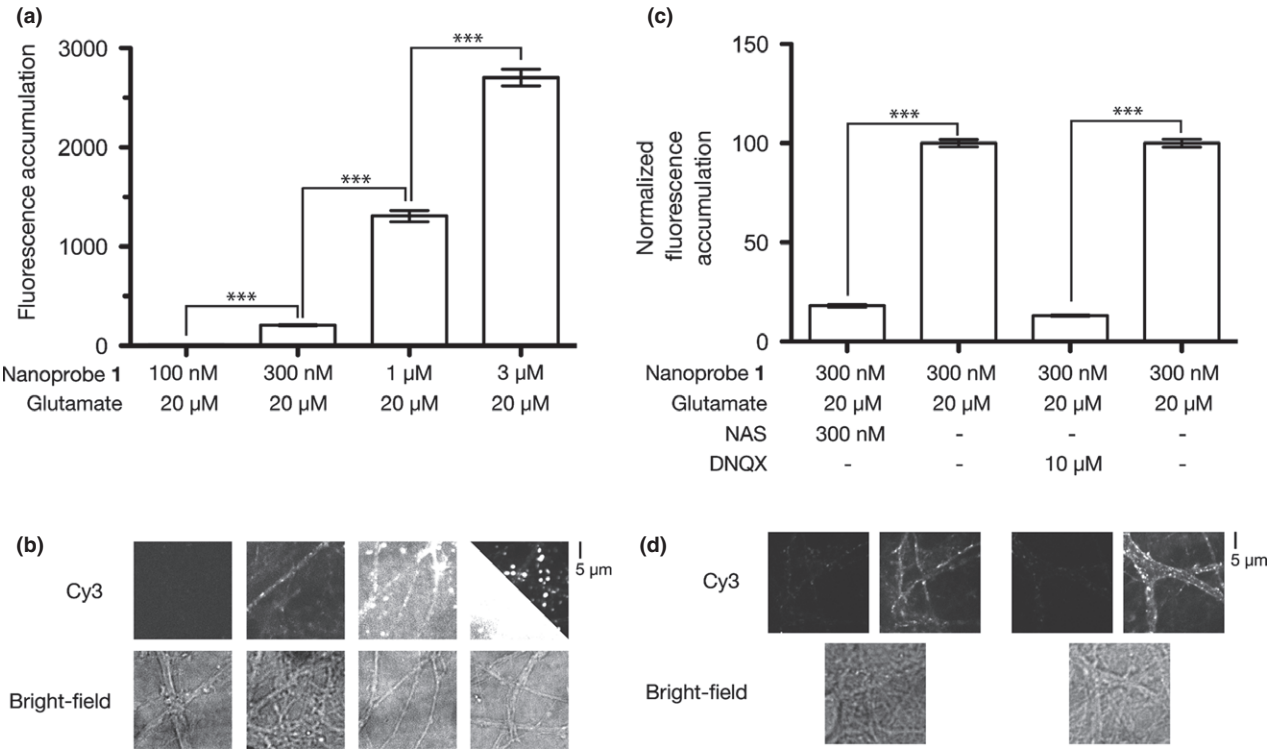

Fig. 2 Nanoprobe **1** covalently labels DIV 14–17 neurons in a concentration-dependent manner and can be blocked by competitive and allosteric antagonists. (a) Fluorescence accumulation at puncta increases with increasing concentration of Nanoprobe **1** application with 20 μM glutamate. Bar graph represents background subtracted group data [9 coverslips for 100 nM (4664 puncta) that were subsequently used for collecting data on 300 nM (1955 puncta), 1 μM (1166 puncta), and 3 μM (1543 puncta), error bars represent 95% confidence intervals, $***p < 0.0001$, one-way ANOVA, Dunn's multiple-comparison test]. (b) Representative paired fluorescence (Cy3) images from (a) and bright-field images are shown below. All brightness and contrast settings are identical with the exception of the top, right half of the 3 μM fluorescence image. The lower, left is depicted at the same brightness and contrast as the other fluorescence images while the top, right is set to show contrast with this high concentration. (c) Fluorescence accumulation can be prevented with co-incubation. Either 300 nM naphthylacetylspermine (NAS) or 10 μM 6,7-dinitroquinoxaline-2,3-dione (DNQX) can significantly prevent 20 μM glutamate and 300 nM Nanoprobe **1** labeling of cells. Bar graph represents background subtracted data that were normalized to peak fluorescence intensity collected 1 min after washing away non-bound Nanoprobe **1** alone (3 coverslips for each condition [1766 puncta for NAS experiment, 2021 puncta for DNQX experiment], error bars represent 95% confidence intervals, $***p < 0.0001$, one-way ANOVA, Dunn's multiple-comparison test). (d) Representative paired fluorescence (Cy3) images from (c) of co-incubation and Nanoprobe **1** alone along with bright-field images are shown below. All brightness and contrast settings are identical.

one of these molecules has been used extensively to specifically target and block CP-AMPARs. However, determining an accurate IC_{50} value for this pharmacological class has been the subject of some effort due to differences in reported neuronal preparation and experimental conditions. Variables such as the age of the neuronal preparation, the use of intact versus dissociated tissue, and the concentration of agent, as well as the use-dependency and voltage-sensitivity of antagonism that these molecules exhibit, have all contributed to a broad range in reported efficacy. Reported IC_{50} values for this class of blockers range from 30 nM to 3 μM (Brackley 1992; Jackson *et al.* 2011) and thus we tested a similar range of concentrations of Nanoprobe **1** to optimize labeling while attempting to maintain specificity.

Dose-dependent labeling of CP-AMPARs in live neurons

To determine an optimal concentration for labeling these receptors with Nanoprobe **1**, coverslips of live neurons at age DIV 14–17 were used because our lab and others have found them to be synaptically active and expressing AMPA receptors (Whitney *et al.* 2008; Bats *et al.* 2013). Since 100 nM Nanoprobe **1** was found to result in very little fluorescence accumulation, we followed those treatments with a higher concentration of the probe that would allow us to highlight spines and determine labeling that occurred with the previous 100 nM incubation. Without doing this low and then higher concentration incubation, it was impossible to quantify the very weak fluorescence imparted by 100 nM of the probe. In brief, the cells on coverslips were washed three times with extracellular buffer, imaged to measure back-

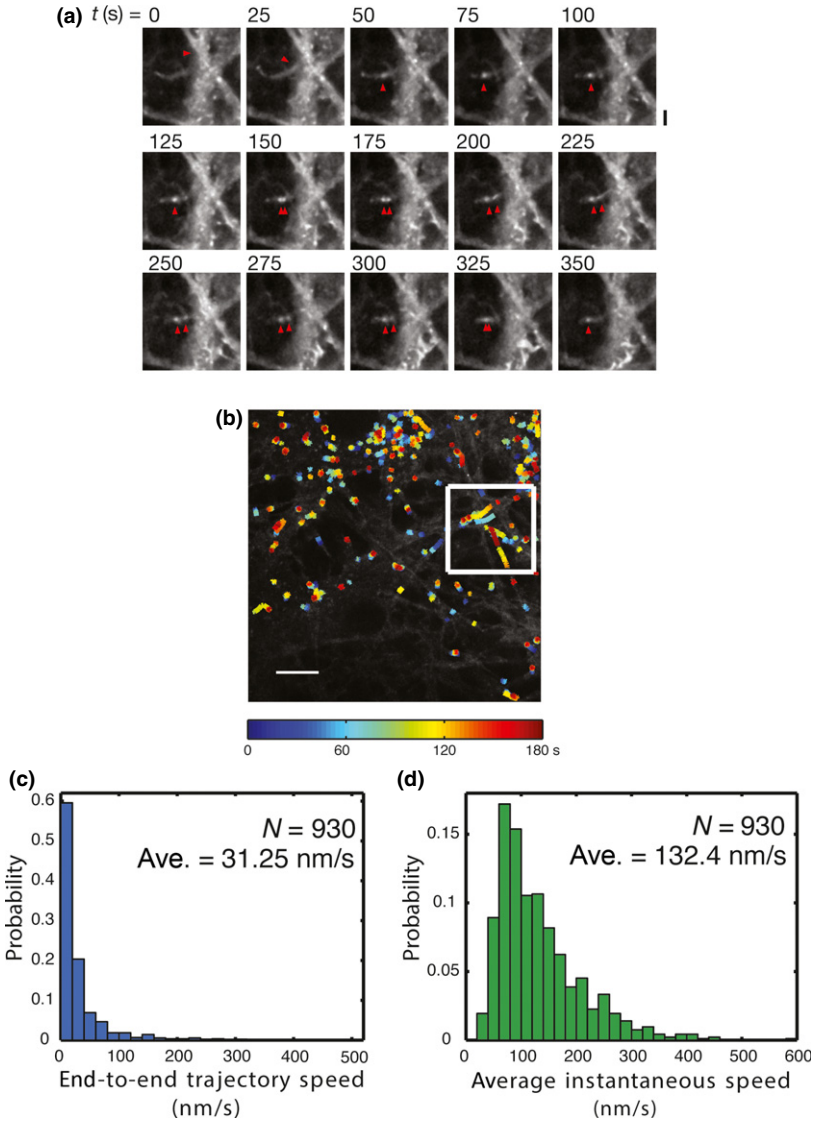

Fig. 3 Movements of Nanoprobe **1**-labeled receptors. (a) Example of a moving cluster indicated by red arrowheads that is delivered to a putative synaptic spine. Time = 0 when the receptor cluster became visible. Scale bar for images is 2 μm long. (b) Overlay of detected trajectories of a number of particles moving along neurites. Colors of tracks indicate time of detection (blue = 0 s, red = 180 s). Scale bar for image is 10 μm long. White box corresponds to Movie S2 in which clusters are highlighted and tracked. (c) Binned histogram of end-to-end trajectory speed of 930 mobile clusters from five separate time-lapse sequences. (d) Binned histogram of instantaneous speed of 930 mobile clusters from five separate time-lapse sequences.

ground fluorescence, and then treated with 20 μM glutamate and 100 nM Nanoprobe **1** in extracellular buffer for 5 min in the dark to prevent premature photolysis. After this incubation period with a low concentration of Nanoprobe **1**, the coverslips were washed three times with extracellular buffer and imaged again to determine accumulated fluorescence induced by 100 nM probe. Next, the same coverslip was used to assay a higher concentration of Nanoprobe **1**, independently assaying 300 nM, 1 μM, or 3 μM in extracellular buffer along with 20 μM glutamate. Again, a 5 min incubation in the higher concentration of Nanoprobe **1** with 20 μM glutamate in the dark was followed by three washes with extracellular buffer prior to resuming imaging. We performed this treatment and imaging regime so that we could compare labeling within a range of concentrations similar to the IC_{50} reports for the pharmacological class on which Nanoprobe **1** is based. We choose 100 nM as our low concentration because previous experiments with 30 nM resulted in no detectable fluorescence accumulation (data not shown).

We found that Nanoprobe **1** concentrations of 100 nM were not statistically different from background fluorescence on any of the neurons we tested (Fig. 2a and b). However, 300 nM Nanoprobe **1** resulted in an increase in fluorescence, with accumulations of peak brightness on neurites in a pattern that appeared to be located at synaptic spines as judged by bright-field density and morphology. Use of Nanoprobe **1** concentrations of 1 or 3 μM demonstrated a marked increase in accumulated fluorescence, however, this labeling appeared to be non-specific in nature. We determined that a 5 min incubation of 300 nM Nanoprobe **1** with 20 μM glutamate in the dark was sufficient for consistent and robust labeling. Thus, 300 nM Nanoprobe **1** with 20 μM glutamate was used for all other experiments described in this manuscript. Through extensive use of 300 nM of this probe, we have observed no evidence during numerous

confocal and wide-field imaging experiments of direct cytoplasmic loading that would occur via diffusion across the neuronal membrane. Nanoprobe **1** has a formal positive charge and thus should not passively cross the cell membrane. The fact that Nanoprobe **1** does end up in vesicles suggests that endocytosis of targeted receptors is occurring rapidly and will be the subject of future studies.

Nanoprobe 1 labeling is prevented by co-incubation with either NAS or DNQX

To test the specificity of our molecule we applied Nanoprobe **1** while co-treating with non-fluorescent competitor molecules. In one series of experiments, we treated neurons with a stoichiometric concentration of NAS in conjunction with our probe to determine if the probe molecule was reacting with off-target proteins or if it was targeting the same ion conduction pore site as NAS. This experiment was performed on live neurons so that we could collect data from before incubation (background fluorescence), after glutamate/Nanoprobe **1**/NAS co-incubation, and then after incubation with glutamate/Nanoprobe **1** alone, washing the cells with extracellular buffer between each treatment regime. We hypothesized that the NAS co-incubation should block some, but not all, of our probe labeling since the two molecules share the acylated polyamine ligand. However, NAS is a non-covalent drug whereas Nanoprobe **1** forms a covalent bond with no off-rate and thus acts as a kinetic trap until photolysis of the nitroindoline releases the ligand. While others have studied kinetic traps by using covalent and non-covalent competition experiments, the two molecules in question here, NAS and Nanoprobe **1**, are both voltage sensitive due to their polycationic nature and, upon binding, do not demonstrate an appreciable off rate (Leung *et al.* 2003). It is likely more useful to think of these two molecules as both non-covalent molecules in the context of a live, hyperpolarized neuron.

We found that the co-incubation of our cells with a combination of 20 μM glutamate, 300 nM Nanoprobe **1,** and 300 nM NAS resulted in a modest increase in fluorescence intensity (18.1% increase) when compared to background fluorescence. However, when we co-treated these same fields of view with a combination of glutamate and Nanoprobe **1** alone, we observed a large increase in fluorescence (providing the maximal, normalized fluorescence in this experiment, 100%). This result suggests that NAS and Nanoprobe **1** compete for the same binding sites (Fig. 2c and d). Since NAS is a non-covalent binder, we expected this stoichiometric competition experiment to result in around 50% labeling of binding sites because Nanoprobe **1** should kinetically trap the binding event. However, the results from this experiment demonstrate that NAS blocks the majority of the fluorescence accumulation of Nanoprobe **1**. The fact that NAS blocks more than 50% of Nanoprobe **1** labeling suggests that the binding affinity of NAS is significantly higher than that of Nanoprobe **1**. A minor concern that we had during the combination of NAS and Nanoprobe **1** experiments was that the NAS was undergoing a covalent modification by the acrylamide on Nanoprobe **1** and this could explain the lack of Nanoprobe **1** accumulation at receptors. However, we have found no evidence that NAS covalently reacts with the Nanoprobe **1** molecule when assayed by LC/MS (data not shown).

To assay the specificity of Nanoprobe **1** for AMPA receptors, we performed another competition experiment with a competitive antagonist for the glutamate-binding site. The Nanoprobe **1** ligand is designed to interact with the intrinsic ion channel conduction pore of CP-AMPARs when the channel is activated. DNQX is known to block the glutamate-binding site of AMPARs and kainate receptors, and is expected to prevent channel opening. Thus, we expected co-incubation with 10 μM DNQX to prevent fluorescent labeling with 20 μM glutamate and 300 nM Nanoprobe **1**. Indeed, when we co-treated DIV 14–17 neurons with a combination of DNQX, glutamate, and Nanoprobe **1,** we found a slight increase in fluorescence intensity (13.1% increase) when compared to background fluorescence (Fig. 2c). Gratifyingly, however, when we co-treated these same fields of view with a combination of 20 μM glutamate and 300 nM Nanoprobe **1** alone, we observed a large increase in fluorescence (providing the maximal, normalized fluorescence in this experiment, 100%). Similar to the previously described experiment, after the glutamate/Nanoprobe **1**/DNQX co-treatment, coverslips were washed and treated with 20 μM glutamate and 300 nM Nanoprobe **1** alone. This resulted in a marked increase in fluorescence intensity and suggests that Nanoprobe **1** labeling is dependent on probe specificity for glutamate receptors that are sensitive to DNQX antagonism. The DNQX data combined with the block of fluorescence accumulation demonstrated by co-treatment with NAS suggest that the target of Nanoprobe **1** labeling is indeed NAS sensitive glutamate receptors and are very likely CP-AMPARs.

Tracked movements of Nanoprobe 1-labeled receptors

One of the motivations for the development of a traceless, chemical-based method to label CP-AMPARs was to observe minimally perturbed receptor movement in live neurons. To accomplish this goal, we recorded time-lapse images of neurons that were labeled with Nanoprobe **1** and we expected to observe movements of these labeled receptors undergoing local lateral diffusion as well as intracellular vesicular trafficking.

To visualize receptor labeling and trafficking in neuronal cultures, live cells (DIV 14–17) were washed with extracellular buffer and incubated with 20 μM glutamate and 300 nM Nanoprobe **1** for 5 min in the dark, exposed to 405 nm light for photolysis of the nitroindoline, washed again, and imaged to compile a time-series. We found

numerous examples of both stable spots of fluorescence and of receptor clusters that moved either locally or comparatively long distances along a neurite and, at times, across the entire field of view (Movie S1 is demonstrative of these diverse movements and Movie S2 is a sub-region of Movie S1 that contains colored lines to demonstrate the detected movements). The relatively fast moving clusters of receptors traveling along neurites appear to be intracellular and in vesicular packages undergoing active transport based on their common movement paths. The velocities of the clustered movements that we observed are consistent with intracellular vesicular transport observed in normal neurons (Turina *et al.* 2011; Ahmed *et al.* 2013). The vesicular packages of AMPA receptors have been reported elsewhere and the movements we observe here closely resemble the trafficking that others have observed for fluorescently-tagged glutamate receptor subunits in vesicles (Washbourne *et al.* 2002; Ju *et al.* 2004).

We found that the labeled receptors in vesicles move at a fairly wide range of mean velocities (Fig. 3) with two groups appearing from the particle tracking analysis. Some of these clusters move very quickly along tracks defined by neurites while others remain stationary, appearing to undergo thermal or non-active motion during imaging. After quantifying the mean velocity of 930 moving particles from five independent time-lapse experiments, we found that the mean end-to-end velocity of these clusters is 31.25 nm/s and a mean instantaneous velocity of 132.4 nm/s. The end-to-end velocity is a measure of overall movement where the instantaneous velocity provides information on the full range of velocity experienced by individual particles.

In addition to the movement of vesicular-located receptors along neurites, we also observed receptors in vesicles being delivered to a putative synaptic spine (Fig. 3a and Movie S3). We believe that these labeled receptors were expressed on the surface where they were labeled with our probe prior to endocytosis during the 5 min incubation period and then recycled. Because the probe does not cross the membrane unassisted, we can surmise that these fluorophores are appended to previously exposed CP-AMPARs.

The observed movements of labeled receptors are consistent with the previously reported velocities for tracking of NMDA, GluA1, and GluA2 receptor subunits. Our results match quite closely previous reports in which fluorescent fusion protein subunits were tracked in either dissociated cortical cultures at DIV 3–4 (Washbourne *et al.* 2002) or in dissociated hippocampal cultures at DIV 8–9 (Ju *et al.* 2004). By using Nanoprobe **1** to label these receptors, we found an average end-to-end velocity of about 31 nm/s, which is almost identical to the velocity observed for both NR1 alone and NR1/GluA1 clusters combined (Washbourne *et al.* 2002) and to that observed for GluA1 and GluA2 clusters (Ju *et al.* 2004). Thus, our observations of very similar intracellular trafficking velocities suggest that our labeling methodology is comparable to sometimes complex genetically engineered methods used for observing receptor movement.

In addition to intracellular movements of labeled receptors, we have also observed that areas of strong Nanoprobe **1** labeling can be found to migrate locally in response to excitatory stimuli. In some cases, during global bath application of glutamate to Nanoprobe **1**-labeled neurons, we observed the movement of labeled receptors into putative synaptic spines (Fig. 4a and b). Further study of this effect will be carried out in acute slices where synapse organization is more predictable than that found in dissociated culture.

Discussion

AMPA receptors are the main receptors for excitatory neurotransmission in the CNS, are believed to play a key role in synaptic plasticity, and have been implicated in several neuropathological diseases. Thus, the locations, movements, and interactions of endogenous AMPA receptors throughout development and under different metabolic or stimulation conditions are topics of interest. Despite a decade of work, visual strategies to follow the movements of these receptors still rely on the use of genetic engineering or antibodies. While these strategies are exquisitely specific towards the proteins of interest, perturbations in natural movement have been observed. Additionally, these methods are not typically capable of distinguishing the subunit composition of heteromultimeric ion channels. Our Nanoprobe **1** molecule complements the features of traditional methods of receptor visualization, but offers new insight by targeting the receptor phenotype of interest in a minimally perturbing manner.

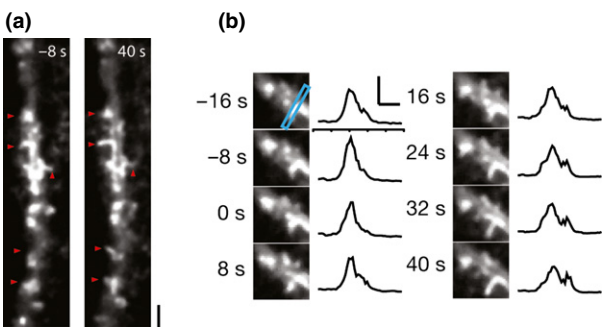

Fig. 4 Local movements of fluorescence into spines. (a) Spine dynamics observed as Nanoprobe **1**-labeled receptors move into spine heads. This culture was labeled with Nanoprobe **1** and then stimulated with glutamate at time = 0 s. Red arrows point to areas of labeled receptor movement into putative spines. Scale bar is 2.0 μm. (b) Fluorescence profile of one spine (indicated by blue rectangle) from (a) demonstrating the movement of receptors into the spine. Scale bar; x = 1.0 μm, y = 500 AU.

Nanoprobe **1** was developed to provide a simple and minimally-perturbing method for the rapid and targeted labeling of active CP-AMPARs on live tissue. Delivery of the fluorophore provides information about both receptor phenotype and the activity of the receptor during the time of labeling. The ligand, an acylated polyamine, is thought to interact with the ion conduction pore of CP-AMPARs where it halts ion flow (Nelson *et al.* 2009). Our method allows us to detect the CP-AMPAR subtype in the milieu of other AMPARs expressed in neurons. Targeting specificity of the probe for active receptors is a result of the open channel blocker connected to the molecule which interacts with the ion channel pore when the receptor is open.

The ligand-directed Nanoprobe **1** also bears a promiscuous electrophilic group for covalent bond formation with an amino acid side-chain on the ion channel. Bioconjugation of this molecule results in a new covalent bond between the probe molecule and the target receptor, after which photolysis of the nitroindoline portion of the molecule may be activated to effect ligand release. Photolysis returns the covalently tagged receptor to the non-antagonized state while retaining the fluorescent beacon for visualization using live cell fluorescence microscopy. It is important to relieve persistently activated or antagonized receptors to avoid ligand-induced trafficking. Both agonist-induced and antagonist-induced conformational changes of some receptors, including glutamate receptors, have been shown to induce clathrin-mediated endocytosis as well as differential trafficking (Lin *et al.* 2000; Malinow *et al.* 2005; Gonzalez-Maeso and Sealfon 2009; Digby *et al.* 2010; Lalo *et al.* 2010; Terunuma *et al.* 2010). Our probe circumvents this potential problem by decoupling the ligand from the remainder of the probe after delivery via a short pulse of light.

While we cannot presently conclude that Nanoprobe **1** is completely selective for CP-AMPARs, it does label NAS-sensitive surface proteins on native neurons in a dose-dependent manner and labeling can be prevented by co-incubation with either the non-NMDA glutamate receptor antagonist DNQX or the parent pharmacophore NAS. These proteins, once labeled, can be tracked over time, allowing us to observe both their local movements and their travel along neurite shafts and their delivery to synaptic spines. In DIV 14–17 neurons we measured an average velocity for these receptors that agrees with previously reported data collected on labeled glutamate receptor subunits. The effectiveness of the NAS competitive blockade during co-incubation indicates that Nanoprobe **1** shares target specificity with NAS, very likely the ion conduction pore of these CP channels. We were surprised to observe the relative abundance of labeling when using Nanoprobe **1** on hippocampal neurons during live imaging experiments, and this finding could suggest that these cells express more CP-AMPARs than previously thought, that there are more NAS targets that are also sensitive to DNQX block, or both. It should be noted that NAS and the other naturally occurring polyamine toxins are currently some of the main pharmacological tools used to specifically target and study CP-AMPARs. The question of definitive target identity remains open and is the subject of future studies. A new probe molecule that will allow irrefutable biochemical and proteomic identification of the targets for these types of probes is well underway.

Acknowledgments and conflict of interest disclosure

We thank P. Wadsworth, J. Ross, and S. Balchand for very helpful discussions and advice on image acquisition and analysis. The spinning disk confocal instrument was part of an MRI grant from NSF: NSF-DBI: 0923318. This work was funded by the University of Massachusetts, Amherst.

All experiments were conducted in compliance with the ARRIVE guidelines.

Supporting information

Additional supporting information may be found in the online version of this article at the publisher's web-site:

Movie S1. Movements of Nanoprobe **1**-labeled receptors in non-stimulated neurons.

Movie S2. Zoomed area of Movie 1 showing trajectory development and tracking.

Movie S3. Delivery of putative recycling endocytic vesicle-containing Nanoprobe **1**-labeled receptors to a synaptic spine.

Data S1. Captions for supplemental movies.

References

Ahmed W. W., Williams B. J., Silver A. M. and Saif T. A. (2013) Measuring nonequilibrium vesicle dynamics in neurons under tension. *Lab Chip* **13**, 570–578.

Bats C., Farrant M. and Cull-Candy S. G. (2013) A role of TARPs in the expression and plasticity of calcium-permeable AMPARs: evidence from cerebellar neurons and glia. *Neuropharmacology* **74**, 76–85.

Bennett M. V., Pellegrini-Giampietro D. E., Gorter J. A., Aronica E., Connor J. A. and Zukin R. S. (1996) The GluR2 hypothesis: Ca (++)-permeable AMPA receptors in delayed neurodegeneration. *Cold Spring Harb. Symp. Quant. Biol.* **61**, 373–384.

Bogaert E., d'Ydewalle C. and Van Den Bosch L. (2010) Amyotrophic lateral sclerosis and excitotoxicity: from pathological mechanism to therapeutic target. *CNS Neurol. Disord. Drug Targets* **9**, 297–304.

Brackley M. H. (1992) A role supplementation group pilot study: a nursing therapy for potential parental caregivers. *Clin. Nurse Spec.* **6**, 14–19.

Chambers J. J. and Kramer R. H. (2008) Light-activated ion channels for remote control of neural activity. *Methods Cell Biol.* **90**, 217–232.

Corona J. C. and Tapia R. (2007) Ca^{2+}-permeable AMPA receptors and intracellular Ca2+ determine motoneuron vulnerability in rat spinal cord *in vivo*. *Neuropharmacology* **52**, 1219–1228.

Corona J. C., Tovar-y-Romo L. B. and Tapia R. (2007) Glutamate excitotoxicity and therapeutic targets for amyotrophic lateral sclerosis. *Expert Opin. Ther. Targets* **11**, 1415–1428.

Cull-Candy S., Kelly L. and Farrant M. (2006) Regulation of Ca2+-permeable AMPA receptors: synaptic plasticity and beyond. *Curr. Opin. Neurobiol.* **16**, 288–297.

Digby G. J., Conn P. J. and Lindsley C. W. (2010) Orthosteric- and allosteric-induced ligand-directed trafficking at GPCRs. *Curr. Opin. Drug Discov. Devel.* **13**, 587–594.

Gonzalez-Maeso J. and Sealfon S. C. (2009) Agonist-trafficking and hallucinogens. *Curr. Med. Chem.* **16**, 1017–1027.

Hideyama T., Yamashita T., Nishimoto Y., Suzuki T. and Kwak S. (2010) Novel etiological and therapeutic strategies for neurodiseases: RNA editing enzyme abnormality in sporadic amyotrophic lateral sclerosis. *J. Pharmacol. Sci.* **113**, 9–13.

Isaac J. T., Ashby M. C. and McBain C. J. (2007) The role of the GluR2 subunit in AMPA receptor function and synaptic plasticity. *Neuron* **54**, 859–871.

Jackson A. C., Milstein A. D., Soto D., Farrant M., Cull-Candy S. G. and Nicoll R. A. (2011) Probing TARP modulation of AMPA receptor conductance with polyamine toxins. *J. Neurosci.* **31**, 7511–7520.

Ju W., Morishita W., Tsui J. *et al.* (2004) Activity-dependent regulation of dendritic synthesis and trafficking of AMPA receptors. *Nat. Neurosci.* **7**, 244–253.

Kerchner G. A. and Nicoll R. A. (2008) Silent synapses and the emergence of a postsynaptic mechanism for LTP. *Nat. Rev. Neurosci.* **9**, 813–825.

Kwak S., Hideyama T., Yamashita T. and Aizawa H. (2010) AMPA receptor-mediated neuronal death in sporadic ALS. *Neuropathology* **30**, 182–188.

Lalo U., Allsopp R. C., Mahaut-Smith M. P. and Evans R. J. (2010) P2X1 receptor mobility and trafficking; regulation by receptor insertion and activation. *J. Neurochem.* **113**, 1177–1187.

Lee S., Yang G., Yong Y. *et al.* (2010) ADAR2-dependent RNA editing of GluR2 is involved in thiamine deficiency-induced alteration of calcium dynamics. *Mol. Neurodegener.* **5**, 54.

Leung D., Hardouin C., Boger D. L. and Cravatt B. F. (2003) Discovering potent and selective reversible inhibitors of enzymes in complex proteomes. *Nat. Biotechnol.* **21**, 687–691.

Lin J. W., Ju W., Foster K., Lee S. H., Ahmadian G., Wyszynski M., Wang Y. T. and Sheng M. (2000) Distinct molecular mechanisms and divergent endocytotic pathways of AMPA receptor internalization. *Nat. Neurosci.* **3**, 1282–1290.

Liu S. J. and Zukin R. S. (2007) Ca2+-permeable AMPA receptors in synaptic plasticity and neuronal death. *Trends Neurosci.* **30**, 126–134.

Liu S., Lau L., Wei J., Zhu D., Zou S., Sun H. S., Fu Y., Liu F. and Lu Y. (2004) Expression of Ca(2+)-permeable AMPA receptor channels primes cell death in transient forebrain ischemia. *Neuron* **43**, 43–55.

Malinow R., Rumpel S., Zador A. and Ledoux J. (2005) AMPA receptor trafficking and GluR1 - Response. *Science* **310**, 234–235.

Mangiavacchi S. and Wolf M. E. (2004) D1 dopamine receptor stimulation increases the rate of AMPA receptor insertion onto the surface of cultured nucleus accumbens neurons through a pathway dependent on protein kinase A. *J. Neurochem.* **88**, 1261–1271.

Morita D., Rah J. C. and Isaac J. T. (2014) Incorporation of inwardly rectifying AMPA receptors at silent synapses during hippocampal long-term potentiation. *Philos. Trans. R. Soc. Lond. B Biol. Sci.* **369**, 20130156.

Nelson J. K., Frolund S. U., Tikhonov D. B., Kristensen A. S. and Stromgaard K. (2009) Synthesis and biological activity of argiotoxin 636 and analogues: selective antagonists for ionotropic glutamate receptors. *Angew. Chem. Int. Ed. Engl.* **48**, 3087–3091.

Pelletier V., Gal N., Fournier P. and Kilfoil M. L. (2009) Microrheology of microtubule solutions and actin-microtubule composite networks. *Phys. Rev. Lett.* **102**, 188303.

Rajasekaran K., Todorovic M. and Kapur J. (2012) Calcium-permeable AMPA receptors are expressed in a rodent model of status epilepticus. *Ann. Neurol.* **72**, 91–102.

Ribrault C., Sekimoto K. and Triller A. (2011) From the stochasticity of molecular processes to the variability of synaptic transmission. *Nat. Rev. Neurosci.* **12**, 375–387.

Sanderson J. L., Gorski J. A., Gibson E. S., Lam P., Freund R. K., Chick W. S. and Dell'Acqua M. L. (2012) AKAP150-anchored calcineurin regulates synaptic plasticity by limiting synaptic incorporation of Ca2+-permeable AMPA receptors. *J. Neurosci.* **32**, 15036–15052.

Schneider C. A., Rasband W. S. and Eliceiri K. W. (2012) NIH Image to ImageJ: 25 years of image analysis. *Nat. Methods* **9**, 671–675.

Spaethling J., Le L. and Meaney D. F. (2012) NMDA receptor mediated phosphorylation of GluR1 subunits contributes to the appearance of calcium-permeable AMPA receptors after mechanical stretch injury. *Neurobiol. Dis.* **46**, 646–654.

Stromgaard K. and Mellor I. (2004) AMPA receptor ligands: synthetic and pharmacological studies of polyamines and polyamine toxins. *Med. Res. Rev.* **24**, 589–620.

Stromgaard K., Brierley M. J., Andersen K., Slok F. A., Mellor I. R., Usherwood P. N. R., Krogsgaard-Larsen P. and Jaroszewski J. W. (1999) Analogues of neuroactive polyamine wasp toxins that lack inner basic sites exhibit enhanced antagonism toward a muscle-type mammalian nicotinic acetylcholine receptor. *J. Med. Chem.* **42**, 5224–5234.

Szabo A., Somogyi J., Cauli B., Lambolez B., Somogyi P. and Lamsa K. P. (2012) Calcium-permeable AMPA receptors provide a common mechanism for LTP in glutamatergic synapses of distinct hippocampal interneuron types. *J. Neurosci.* **32**, 6511–6516.

Tateno M., Sadakata H., Tanaka M. *et al.* (2004) Calcium-permeable AMPA receptors promote misfolding of mutant SOD1 protein and development of amyotrophic lateral sclerosis in a transgenic mouse model. *Hum. Mol. Genet.* **13**, 2183–2196.

Terunuma M., Pangalos M. N. and Moss S. J. (2010) Functional modulation of GABAB receptors by protein kinases and receptor trafficking. *Adv. Pharmacol.* **58**, 113–122.

Trigo F. F., Corrie J. E. and Ogden D. (2009) Laser photolysis of caged compounds at 405 nm: photochemical advantages, localisation, phototoxicity and methods for calibration. *J. Neurosci. Methods* **180**, 9–21.

Turina D., Bjornstrom K., Sundqvist T. and Eintrei C. (2011) Propofol alters vesicular transport in rat cortical neuronal cultures. *J. Physiol. Pharmacol.* **62**, 119–124.

Vytla D., Combs-Bachmann R. E., Hussey A. M., Hafez I. and Chambers J. J. (2011) Silent, fluorescent labeling of native neuronal receptors. *Org. Biomol. Chem.* **9**, 7151–7161.

Washbourne P., Bennett J. E. and McAllister A. K. (2002) Rapid recruitment of NMDA receptor transport packets to nascent synapses. *Nat. Neurosci.* **5**, 751–759.

Whitney N. P., Peng H., Erdmann N. B., Tian C., Monaghan D. T. and Zheng J. C. (2008) Calcium-permeable AMPA receptors containing Q/R-unedited GluR2 direct human neural progenitor cell differentiation to neurons. *FASEB J.* **22**, 2888–2900.

Wolf M. E. and Tseng K. Y. (2012) Calcium-permeable AMPA receptors in the VTA and nucleus accumbens after cocaine exposure: when, how, and why? *Front. Mol. Neurosci.* **5**, 72.

Yoneda Y., Kawajiri S., Hasegawa A., Kito F., Katano S., Takano E. and Mimura T. (2001) Synthesis of polyamine derivatives having non-hypotensive Ca2 +-permeable AMPA receptor antagonist activity. *Bioorg. Med. Chem. Lett.* **11**, 1261–1264.

Yuan T. and Bellone C. (2013) Glutamatergic receptors at developing synapses: the role of GluN3A-containing NMDA receptors and GluA2-lacking AMPA receptors. *Eur. J. Pharmacol.* **719**, 107–111.

Yuan T., Mameli M., O'Connor E. C., Dey P. N., Verpelli C., Sala C., Perez-Otano I., Luscher C. and Bellone C. (2013) Expression of cocaine-evoked synaptic plasticity by GluN3A-containing NMDA receptors. *Neuron* **80**, 1025–1038.

Zack G. W., Rogers W. E. and Latt S. A. (1977) Automatic measurement of sister chromatid exchange frequency. *J. Histochem. Cytochem.* **25**, 741–753.

Zonouzi M., Renzi M., Farrant M. and Cull-Candy S. G. (2011) Bidirectional plasticity of calcium-permeable AMPA receptors in oligodendrocyte lineage cells. *Nat. Neurosci.* **14**, 1430–1438.